Bayesian Data Assimilation of Acoustically-Forced Laminar Premixed Conical Flames

Alessandro Giannotta*, Matthew Yoko, Stefania Cherubini, Pietro De Palma, Matthew P. Juniper
*alessandro.giannotta@poliba.it

Abstract
We perform experiments on an acoustically-forced laminar premixed conical flame and assimilate experimental flame position data into a physics-based premixed flame model. The experimental rig is a ducted conical flame supplied by a mixture of methane and ethylene. A high-speed camera captures the dynamics of the perturbed flame, as well as snapshots of the stable flame. We model the flame with a front-tracking solver with an imposed velocity field. We use adjoint-accelerated Bayesian inference to identify the most probable model parameters, given the data. Through this, we create a quantitatively-accurate model with quantified uncertainty bounds. The trained model grants access to unmeasured quantities, such as the fluctuating heat release rate, which cannot be reliably deduced solely from flame emission. This study presents a novel method that combines flame natural emissions with reduced-order models to derive the flame transfer function with uncertainty bounds.

1. Introduction
The efficiency of the mechanism driving thermoacoustic oscillations depends strongly on the phase difference between the heat release rate (h.r.r) and pressure oscillations [1]. Because the phase difference is sensitive to small changes in most parts of a thermoacoustic system, its thermoacoustic behaviour tends to be extremely sensitive to small changes [2]. For the same reason, the outputs of faithful thermoacoustic models are also sensitive to small changes in the model parameters or the models themselves. On the positive side, this means that model parameters tend to be observable from data. In other words, with well chosen experiments, we can (i) tune the parameters of candidate models and (ii) compare candidate models against each other and select the best one [3, 4]. This extreme sensitivity also means that thermoacoustic systems can often be stabilized by making small changes, which is attractive in industrial settings. The h.r.r. rate is difficult to model or simulate a priori [5] so people often turn to experimental measurements. Unfortunately, the fluctuating emission from the flame is not a reliable method for measuring the fluctuating h.r.r. [6]. Alternatives, such as PLIF to identify reaction zones [7] are possibly more accurate but are technically difficult and, in large systems, impractical. The approach in this paper solves this problem by combining experimental measurements with numerical simulations. The natural emission of the flame may not directly give the h.r.r. but it does provide data about the flame position as a function of time. This data can be combined with candidate physics-based

models of the flame. We infer the model parameters and their uncertainties from the data. This model gives, amongst other things, the h.r.r. fluctuations as a function of the velocity fluctuations. This flame model will then be included within a larger model of the thermoacoustic behaviour of the system, whose other parameters are inferred in the same way [8]. The end result will be a quantitatively-accurate physics-based model of the flame and thermoacoustic systems that is interpretable, trustworthy, and extrapolatable.

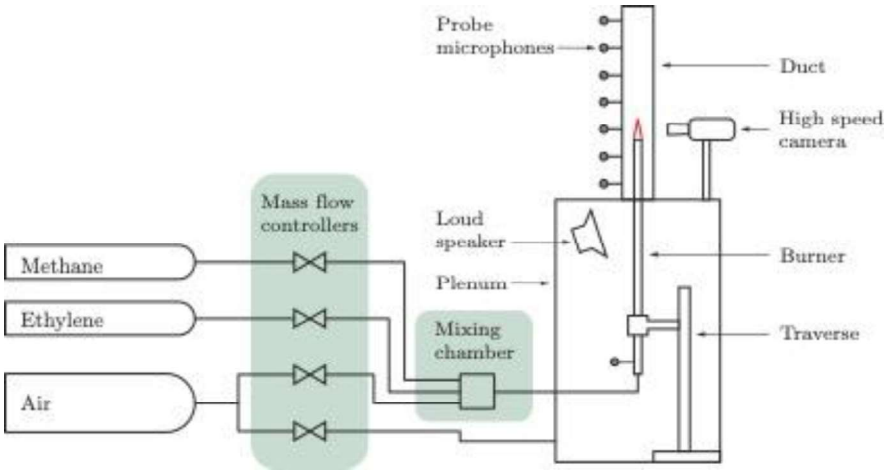

Figure 1. Diagram of the experimental rig.

2. Experiments

The experimental configuration is a laminar premixed conical flame inserted into a vertical duct, as illustrated in Figure 1. The lower end of the duct is fixed to a plenum chamber, through which co-flow air is supplied. The upper end is open to atmosphere. The duct is a 0.8 m long section of quartz tube with an internal diameter of 75 mm. The burner is a 0.85 m long section of brass tubing with an internal diameter of 14 mm. At the injection plane, the nozzle diameter is 9.35 mm. The burner is fuelled by a mixture of methane and ethylene over a wide range of equivalence ratios and fuel mass flow rates. The premixed air and fuel are supplied to the base of the burner via a set of mass flow controllers. A high-speed camera is used to record the flame under both steady and perturbed conditions. The position of the flame-front in the image, is used as the experimental data for data assimilation. The properties of the flame studied in this work are summarised in Table 1. The flame is forced at 230 Hz, which was chosen to be close to the duct's fundamental mode.

Table 1. Summary of the properties of the flame studied in this paper.

Property	Value	Units
Air flow	8.444	[Ln/min]
CH4 flow	0.449	[Ln/min]
C2H4 flow	0.499	[Ln/min]
Equivalence ratio	1.27	[-]

Mean flow velocity	2.45	[m/s]
Mean heat release rate	525	[W]

3. Reduced-Order Model of a laminar premixed Bunsen flame

The flame is approximated by an axisymmetric surface separating the reactants from the products. Each point of the surface is in kinematic equilibrium between the local flame speed and the reactants velocity field. In this study, we adopt a front-tracking method as detailed in Ref [9]. The model can then be expressed compactly through:

$$d\boldsymbol{x}/dt = \boldsymbol{f}(t,\boldsymbol{x};\boldsymbol{p}) \quad (1)$$

where $\boldsymbol{x} = (\boldsymbol{r}, \boldsymbol{z})$ is the state vector defining the flame front position in terms of radial coordinates, $\boldsymbol{r}$, and longitudinal coordinates, $\boldsymbol{z}$. The vector $\boldsymbol{p}$ contains the physics-based parameters, while $\boldsymbol{f}$ is the physics-based nonlinear operator encapsulating the flame-front dynamics. The main feature of the model is that it has been designed to be differentiable with respect to the state and the parameters. The model parameters $\boldsymbol{p}$ are: (i) the flame aspect ratio $\beta = \beta(\bar{u}, S_L)$, which depends on the bulk velocity in the burner tube $\bar{u}$, and the unstretched laminar flame speed S_L; (ii) the nondimensional Markstein length M, which depends on the thermal expansion parameter, the effective Lewis number of the mixture, the Zel'dovich number and the thermal conductivity of the mixture [10]; (iii) the shape parameter μ, which linearly combines a uniform and a parabolic mean velocity profile [11]; (iv) the wavelength of the harmonic perturbation velocity field K; (v) the amplitude of the acoustic forcing ε_V ; (vi) the amplitude of the flame base oscillations λ; (vii) the initial phase of the flame base oscillations φ_0. These seven parameters are sufficient to describe the flame front dynamics qualitatively. All lengths, including the Markstein length, are normalised by the nozzle radius.

4. Bayesian data assimilation

In this section, we introduce the following notation: the data D is the flame position observed in the experiment $\boldsymbol{x_e}$; the model H encodes the reduced-order model described in the previous section such that for a given set of parameters $\boldsymbol{a}$, the model $H(\boldsymbol{a})$ gives a prediction of the flame position $\boldsymbol{x}(\boldsymbol{a})$.

We assume that the model can describe the data and we infer its most probable parameters $\boldsymbol{a_{MP}}$. We propose a prior probability distribution over the parameter values, through which we can encode any prior knowledge. We then use the data, D to perform a Bayesian update on the parameter values:

$$P(\boldsymbol{a}|D,H) = P(D|\boldsymbol{a},H)P(\boldsymbol{a}|H)/P(D|H) \quad (2)$$

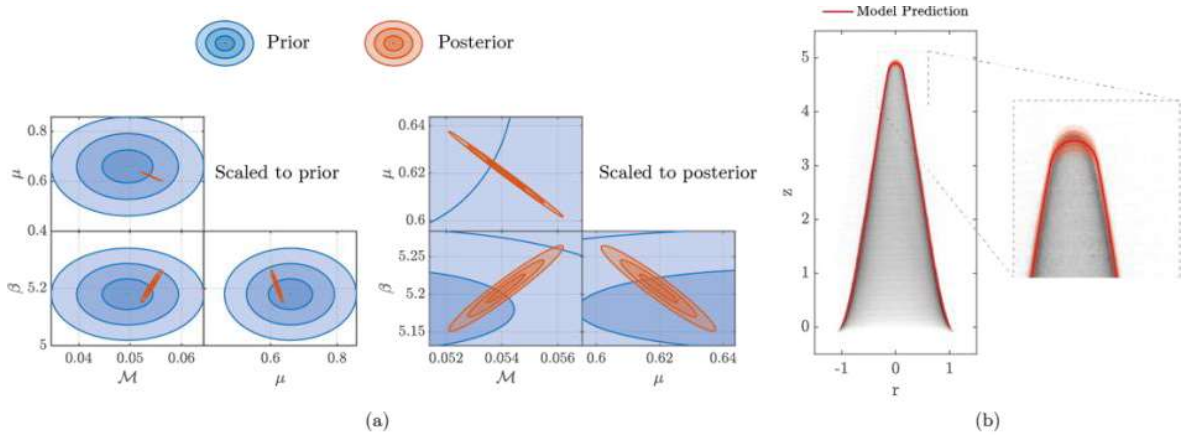

Figure 2. (a) Prior (blue) and posterior (red) probability distributions of the parameters in the steady case. The contours show 1, 2, and 3 standard deviations from the prior and posterior parameter estimations. The parameters are the flame aspect ratio β, the shape parameter for the velocity field μ and the nondimensional Markstein length M. (b) Model prediction (red line) with a confidence interval of 3 standard deviations (red shading) plotted on top of the steady flame image. The panel on the right shows a magnification of the flame tip.

The best estimate of the parameters is that which maximises the left hand side of equation (3). We ignore the denominator because it does not depend on the parameters and we therefore maximise the numerator.
It is convenient to define the cost function, J, as the negative log of the numerator. We then minimise J using a quasi-Newton BFGS method with gradient information provided by adjoint methods. Once we have found the most likely parameters $\boldsymbol{a_{MP}}$, we use Laplace's method [3] to determine their uncertainties. We assume that $P(\boldsymbol{a}|D,H)$ is Gaussian around $\boldsymbol{a_{MP}}$ and approximate the inverse covariance matrix as the Hessian of the cost function.

5. Parameter inference from flame snapshots

The data assimilation process is performed in two steps. From the steady-state flame snapshot we can infer the values of the aspect ratio β, the nondimensional Markstein length M and velocity shape parameter μ. We start by setting a large uncertainty in the prior values of the parameters. Figure 2a shows the prior and posterior probability distribution of the model parameters. The contours show 1, 2 and 3 standard deviations from the prior $\boldsymbol{ap}$ (blue) and posterior $\boldsymbol{a_{MP}}$ (red). In general, the uncertainties in the parameters have been reduced significantly by the data assimilation to quite precise values. Figure 2b shows the model prediction ± 3 standard deviations plotted against the experimental flame-front picture. The largest uncertainties are found at the flame tip, which is the region that is most sensitive to the parameters.
We repeat the process with the images of the acoustically forced flame-front. In this case we use the knowledge gained from the previous step and set large uncertainty in the prior values of K, ε_V, λ and φ_0 . Figure 3 shows the model prediction ± 3

standard deviations, plotted against the experimental flame-fronts, during a limit cycle. As in the steady-state case, the largest uncertainties are found at the flame tip. The discrepancies between the flame-front observations and model predictions are due to model error. This could be reduced by adding more physical phenomena to the model and applying the same data-assimilation process, although this risks creating an elaborate model with too many parameters to be useful. The advantage of the current model is that, even though it contains some model error, it can match the experimental images well at nearly all moments in the cycle. This model, because it contains few parameters, can be trained on a relatively small amount of data.

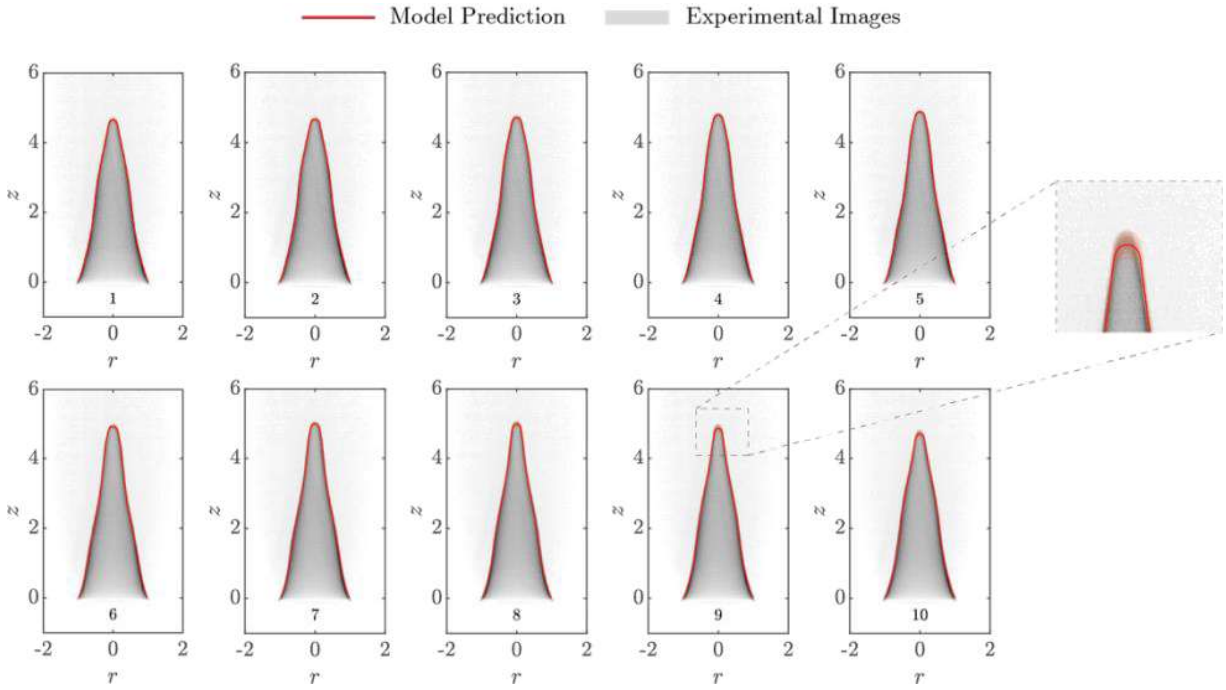

Figure 3. Model prediction (red line) with a confidence interval of 3 standard deviations (red shading) plotted on top of 10 frames of the unsteady flame, captured during a limit cycle.

6. Heat release rate

Once the most probable parameter values are inferred and the flame-front position predictions are obtained, we can estimate the heat release rate. We express the heat release rate, q, as the sum of a steady part, $\bar{q}$, and a perturbation, q'. Figure 4 shows the unsteady heat release rate, q, normalised by the mean heat release rate, $\bar{q}$, plotted over one period. The times at which the snapshots occur are indicated with dots, labelled with the corresponding frame numbers from Figure 3. We see that the trained model allows us to reconstruct a smooth heat release rate signal from sparse observations. We are also able to quantify the uncertainty in the fluctuating heat release rate. Figure 4 also shows the normalised velocity perturbation at the burner rim $u'_Z/\bar{u}$, which gives rise to the heat release rate fluctuations. We are therefore able to use the trained model to quantify the thermoacoustic response of the flame.

For example, by linearising the model around this point, we can calculate the flame transfer function of this flame, with defined uncertainty bounds.

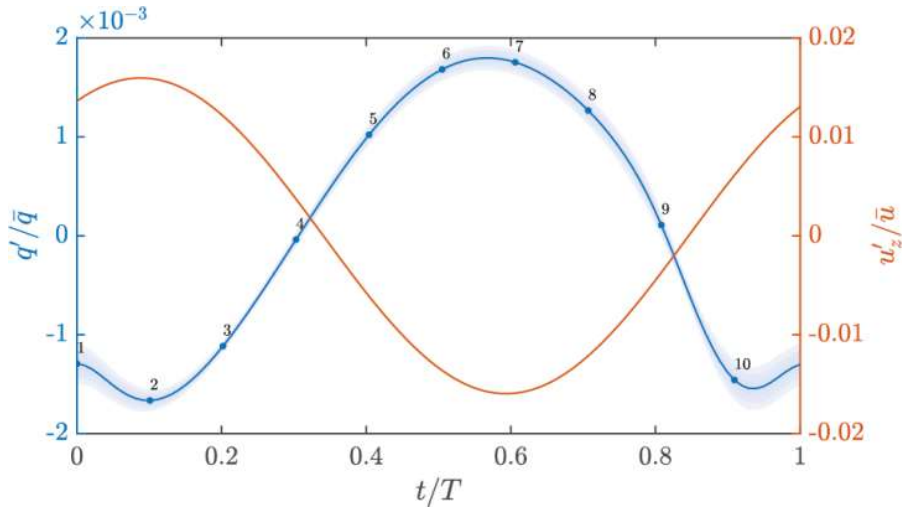

Figure 4. On the left y-axis, we show the normalised heat release rate perturbation, $q'/\bar{q}$, predicted by the model during one period, T, of the limit-cycle (blue line). The numbers on the blue line refer to the frame numbers in Figure 3. The contours show 1, 2, and 3 standard deviations from the maximum a posteriori model prediction. On the right y-axis we show the normalised longitudinal velocity perturbation at the burner rim, $u_z'/\bar{u}$

7. Conclusions

In this study, we perform experiments on an acoustically forced, laminar premixed conical flame in a duct. We use a high-speed camera to record snapshots of the natural emission of the flame while steady and forced. We propose a physics-based reduced-order model of this flame and infer the most probable model parameters from the data. This process (i) turns a qualitatively-accurate model into a quantitatively-accurate model, and (ii) quantifies the uncertainty in the inferred model parameters and the model predictions. The inference process produces a digital-twin of the flame, which provides access to quantities that were not directly measured in the experiments. From observations of the perturbed flame we can infer the fluctuating heat release rate as a response to the velocity perturbation. This is used to calculate the flame's thermoacoustic response through the flame transfer function. We have demonstrated this using snapshots of the natural luminosity of the flame, which can be captured using a basic experimental setup. We can therefore estimate a flame's thermoacoustic response without the need for direct velocity or heat release rate measurements. In future work we will (i) apply this method to a wide range of conical flames, (ii) propose general models for the parameters so that we can predict the behaviour of unseen flames, and (iii) apply the inferred flame transfer functions to a higher level model of the thermoacoustic system.

References

[1] Lieuwen, T. C. and Yang V., "Combustion Instabilities In Gas Turbine Engines: Operational Experience, Fundamental Mechanisms, and Modeling", *volume 210. American Institute of Aeronautics and Astronautics*, 2005.

[2] Mongia H.C., Held T., Hsiao G. and Pandalai R., "Challenges and progress in controlling dynamics in gas turbine combustors". *Journal of Propulsion and Power* 2003; 19(5): 822–829.

[3] Juniper M.P. and Yoko M., "Generating a physics-based quantitatively-accurate model of an electrically-heated Rijke tube with Bayesian inference". *Journal of Sound and Vibration* 2022; 535: 117096.

[4] Yoko M. and Juniper M.P., "Minimizing the data required to train a physics-based thermoacoustic model". In *29th international congress on sound and vibration*, 2023.

[5] Poinsot T., "Prediction and control of combustion instabilities in real engines". *Proceedings of the Combustion Institute* 2017; 36(1): 1–28.

[6] Han Z, Balusamy S and Hochgreb S. "Spatial analysis on forced heat release response of turbulent stratified flames". *Journal of Engineering for Gas Turbines and Power* 2015; 137(6).

[7] Yuan R, Kariuki J, Dowlut A, Balachandran R and Mastorakos E., "Reaction zone visualisation in swirling spray n-heptane flames". *Proceedings of the Combustion Institute* 2015; 35(2): 1649–1656.

[8] Yoko M. and Juniper M.P. "Data-driven modelling of thermoacoustic instability in a ducted conical flame". *In Symposium on Thermoacoustics in Combustion, 11-14 September 2023*, Zurich, Switzerland, pp. 1–12.

[9] Giannotta A., Cherubini S., De Palma P. and Juniper M.P. "The effect of flame curvature and flame base movement on the frequency response of a conical Bunsen flame". *Combustion and Flame*, 2024.

[10] Matalon M. "Intrinsic flame instabilities in premixed and nonpremixed combustion". *Annu Rev Fluid Mech* 2007; 39: 163–191

[11] Yu H, Juniper MP and Magri L. "A data-driven kinematic model of a ducted premixed flame". *Proceedings of the Combustion Institute* 2021; 38(4): 6231–6239.